Pushing the limits of acousto-optics deflectors

Author: Antoni Bericat Vadell
Facultat de Física, Universitat de Barcelona, Diagonal 645, 08028 Barcelona, Spain.

Advisor: Estela Martín Badosa

Abstract: This study investigates the performance and limitations of acousto-optic deflectors by analyzing photon-phonon interactions through a quantum-inspired corpuscular model. The objective is to diffract light homogeneously at N points simultaneously, ensuring uniform intensity distribution across all diffracted orders. A theoretical framework based on Feynman diagrams was developed, offering a detailed understanding of multi-frequency diffraction efficiency. This approach not only accounts for individual photon-phonon interactions but also considers their combined effects under varying acoustic power and frequency distributions. The findings contribute to optimizing light deflection systems, making them more efficient and versatile for advanced photonic applications such as confocal microscopy and holography.

I. INTRODUCTION

Acousto-optic deflectors (AODs) are ultrafast light deflectors that can impart a change in the direction of a laser beam crossing the device at speeds on the order of 100 kHz. Usually, a sinusoidal radio frequency (RF) signal is applied to a piezoelectric transducer bonded to an optical crystal. The vibration of the transducer initiates a sound disturbance in the crystal that spatially modulates the refractive index periodically, creating an internal diffraction grating. Varying the frequency of the control RF signal changes the period of the diffraction grating and thus the laser deflection (Fig. 1).

These devices are typically used in systems for scanning the laser beam on a sample, such as in materials processing or as part of the excitation system in confocal microscopy. When the number of points to be scanned is very large, their extreme speed response loses competitiveness compared to other technologies such as liquid crystal displays or micromechanical systems as DMDs (Digital Micromirror Devices), which are capable of generating hundreds of thousands of points simultaneously.

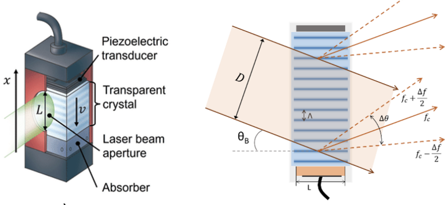

FIG. 1: (a) Structure of an AOD. (b) The induced diffraction grating bends the light at an angle depending on the frequency of the injected sinusoid.

In recent years, the Biophotonics group of the Department of Applied Physics has combined the use of these devices with digital holography techniques to convert them into arbitrary light pattern generators. This is achieved by injecting complex, mathematically designed radiofrequency signals through an arbitrary waveform generator (AWG). The incident laser beam is diffracted into the corresponding synthetic refractive index distributions, thus creating complex light patterns, in contrast to the simple deflection of conventional AODs (Fig. 2).

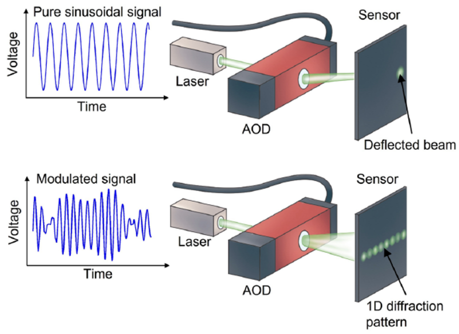

FIG. 2: Sinusoidal RF signal used to deflect light (top). Synthesized signals in which the hologram is encoded (bottom).

In confocal microscopy, the technology developed at the University of Barcelona [1] allows a fluorescent sample to be scanned in parallel, in a programmable way and without mechanical elements. The problem is that, although the acousto-optical interaction inside the crystal is known for an RF signal with a single frequency, the study of the interaction between multiple frequencies when a more generic RF signal is introduced is very complex and has only been carried out theoretically or to explain some very simplified experimental results [2]. These interactions introduce heterogeneities in the deflected light at different directions, which is usually corrected iteratively experimentally [3][4]. The aim of this work is to study an interaction model based on Feynman diagrams in order to optimize the homogeneity of patterns of multiple simultaneous points of light.

A. ACOUSTO-OPTICS DEFLECTORS

In an AOD device, the incident light beam is diffracted through the diffraction grating generated by the acoustic wave propagating in the crystal and, under certain conditions (long length L of interacion), only the first order of diffraction subsists, which satisfies the Bragg condition of constructive interference, i.e.: $2\Lambda \sin\theta_B = \lambda$. Here, Λ is the acoustic wavelength and λ is the wavelength of the light in the medium. Taking into account that the propagation velocity of the acoustic wave v and its frequency f satisfy $v = \Lambda f$, the angle θ_D between the incident and diffracted light is: $\theta_D = 2\theta_B \approx \lambda f/v$.

This means that the diffracted angle is proportional to the frequency f of the RF signal. The $\Delta\theta$ deflection field will be proportional to the frequency range of the system (Δf, bandwidth). The bandwidth and, therefore, the maximum deflection angle, are limited by acousto-optical efficiency. This has two contributions: on one hand, it results from the efficiency in the AO interaction in the crystalline material, when the Bragg condition is satisfied, and, on the other hand, it takes into account what happens when this condition is not strictly satisfied.

Bragg diffraction can be represented graphically in momentum, phase or wave vector space, as shown in Fig. 3. Thus, the relationship between the input beam, the acoustic wave and the output beam derives from the conservation of momentum between the incident $\hbar\mathbf{k}_i$ and diffracted $\hbar\mathbf{k}_d$ photons and the phonon corresponding to the acoustic wave, $\hbar\mathbf{K}_a$, so that $\mathbf{k}_d = \mathbf{k}_i + \mathbf{K}_a$.

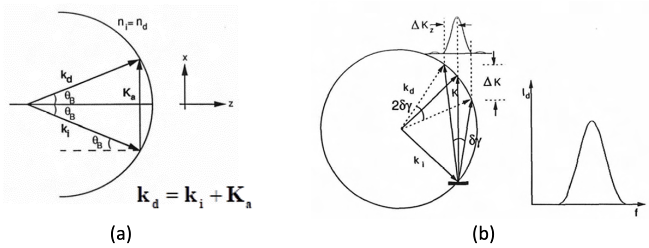

FIG. 3: Isotropic Bragg diffraction: (a) the Bragg condition is satisfied exactly for a single frequency; (b) the angular divergence of the acoustic beam allows other frequencies to match Bragg but with lower intensity, following a $sinc^2$ function.

If, in the diagram in Fig. 3, we vary the acoustic frequency while keeping the light angle of incidence, the acoustic vector length changes and the Bragg condition is no longer satisfied. However, thanks to the finite dimensions L of the transducer, the acoustic wave has a certain divergence and allows the Bragg condition to be satisfied for a set of acoustic wave vectors in directions other than normal to the transducer, although with a lower efficiency, $I_d/I_0 = \text{sinc}^2\left(\frac{\Delta K_z L}{2}\right)$. The 3dB bandwidth Δf is defined as the range of frequencies for which the drop in intensity compared to the maximum I_0 is less than 50%.

II. THEORETICAL MODEL

The Feynman diagram model considers that diffraction is caused by a series of phonon absorptions and emissions by the incident photons. Unlike this model, the coupled-wave model is based on the interaction of light waves with acoustic waves.

The calculations in the quantum model are performed through a postulate. Here, it will not simply be stated but rather inferred from the theoretical results (experimentally verified) of the coupled-wave model.

In what follows, the solutions to the coupled light-sound wave equation are first presented, and subsequently, the correspondences leading to the formulation of the postulate from a quantum perspective are shown.

Three main reinterpretations are made: First, the exponents of the series in the Bessel functions resulting from the wave model will be interpreted as the number of vertices (the total number of phonon emissions and absorptions). Likewise, the base of these powers ($v/2$) will indicate the intensity of the photon-phonon interaction. Second, the part that involves factorials will correspond to the combinations of the different vertices. Third, the parameter t will be interpreted as the total number of emissions.

A. RAMAN-NATH REGIME

For small interaction lengths L we are in the so-called Raman-Nath regime, for which the solution of the differential equation allows diffraction at different orders other than the 0-th and first orders found in the Bragg regime. The diffraction amplitude of the G order of diffraction is given by the Bessel functions [2]:

$$\Psi_G = J_m(v) = \sum_{t=0}^{\infty} \frac{(-1)^t}{t!(t+m)!} \left(\frac{v}{2}\right)^{2t+m} \tag{1}$$

Here, t is an integer parameter, and $2t+m$ is the exponent of the series.

Let us make three reinterpretations with the quantum model:

1. $2t + m = P$ will represent the total number of phonon emissions and absorptions, where t is the number of emissions, and m is the number of absorptions (p) minus the number of emissions: $m = p - t$.
2. The factorials that appear will be interpreted as the combination of the different vertices (points in the diagram where the photon-phonon interaction occurs):

$$\frac{P!}{t!p!} = \frac{(2t+m)!}{t!(t+m)!} \tag{2}$$

Note that the term $(2t+m)!$ does not appear in the solution of the coupled-wave equation. Therefore, the following modification is introduced:

$$\frac{1}{P!}\frac{P!}{t!p!} = \frac{1}{P!}\frac{(2t+m)!}{t!(t+m)!} \tag{3}$$

3.The term $(-1)^t$ will be introduced in the AO interaction theory, with its interpretation being that an even number of emissions (t) contributes positively to the scattering amplitude. With all of this, the postulate is formulated as follows:

$$\Psi_G^{(P)} = \frac{(-1)^t}{P!}\frac{(2t+m)!}{t!(t+m)!}\left(\frac{v}{2}\right)^{2t+m} \tag{4}$$

The superscript (P) refers to the term of the series, corresponding as before to the number of emissions plus the number of absorptions: $P = p + t = 2t + m$.

1. *Example of a Feynman path*

We will analyze one example to gain a better understanding of how the postulate works. Let's consider the path $\{1,\ \bar{1},\ 1\}$: 1 corresponds to the absorption of a phonon, and $\bar{1}$ to its emission.

$$\left.\begin{array}{l}\mathrm{P} = \mathrm{p}+\mathrm{t} = 3\\ \mathrm{m} = \mathrm{p}-\mathrm{t} = 1\end{array}\right\} P = 2\mathrm{t}+\mathrm{m} = 3 \tag{5}$$

$$M^{R-N} = \frac{P!}{t!p!} = \frac{(2t+m)!}{t!(t+m)!} = \frac{(2\cdot 1+1)!}{1!(1+1)!} = 3 \tag{6}$$

$$\Psi_1^{(3)} = \frac{(-1)^1}{3!}3\left(\frac{\nu}{2}\right)^3 = -\frac{1}{2}\left(\frac{\nu}{2}\right)^3 \tag{7}$$

where M^{R-N} is the number of allowed combinations for the given initial and final states, in the $R-N$ regime.

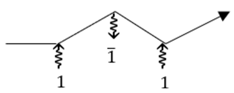

FIG. 4: Representation of the vertices in the Feynman model.

B. BRAGG REGIME

For a single frequency and in the Bragg regime, the solution of the coupled-wave model is [2]:

$$\Psi_G = \sum_{t=0}^{\infty}\frac{(-1)^t}{(2t+m)!}\left(\frac{\nu}{2}\right)^{2t+m} \tag{8}$$

A clear difference is observed with Feynman's postulate in the factorial term. In order for it to match, it must be modified from the previous equation (4) to reach (8) as follows:

$$\Psi_G^{(P)} = \frac{(-1)^t}{P!}\frac{(2t+m)!}{t!(t+m)!}\frac{t!(t+m)!}{(2t+m)!}\left(\frac{v}{2}\right)^{2t+m} \tag{9}$$

Comparing equations (9) and (4) we see that the number of combinations in the Bragg regime, M^B is related to M^{R-N} by:

$$M^B = M^{R-N}\frac{t!(t+m)!}{(2t+m)!} \equiv M^{R-N}q(P,G) \tag{10}$$

This indicates that the combinations are reduced in the Bragg regime with respect to the R-N regime, as only 0-th order and first order diffracted states are allowed.

C. SOLUTION FOR MULTIFREQUENCIES

1. *COUPLED-WAVE EQUATION*

Generalizing for N frequencies:

$$\Psi_G = \prod_{i=1}^{N} J_{m_i}(v_i) = \prod_{i=1}^{N}\sum_{t=0}^{\infty}\frac{(-1)^{t_i}}{t_i!\,(t_i+m_i)!}\left(\frac{v_i}{2}\right)^{2t_i+m_i} \tag{11}$$

If we group by powers of P:

$$\Psi^P = (-1)^t\sum_C\left[\prod_{i=1}^{N}\frac{1}{t_i!\,(t_i+m_i)!}\right]\prod_{i=1}^{N}\left(\frac{v_i}{2}\right)^{2t_i+m_i} \tag{12}$$

$$P = \sum_{i=1}^{N}(2t_i+m_i) = 2\sum_{i=1}^{N}t_i + \sum_{i=1}^{N}m_i = 2t+G \tag{13}$$

Where t and G are the sum of all the t_i and m_i for all the N frequencies, respectively. From here on, $\sum_c$ will be used for those summations that satisfy: $P = 2\sum_{i=1}^{N}t_i + \sum_{i=1}^{N}m_i$.

2. *FEYNMAN DIAGRAM THEORY*

R-N Regime:

$$\Psi^P = \frac{(-1)^t}{P!}\sum_C\left[\prod_{i=1}^{N}\frac{P!}{t_i!\,(t_i+m_i)!}\right]\prod_{i=1}^{N}\left(\frac{v_i}{2}\right)^{2t_i+m_i} \tag{14}$$

$$\mathrm{M}^{R-N} = \prod_{i=1}^{N}\frac{(2t+G)!}{t_i!\,(t_i+m_i)!} \tag{15}$$

Bragg Regime:

$$\Psi^{(P)} = \frac{(-1)^t}{P!}\left[\sum_C M^B\right]\prod_{i=1}^{N}\left(\frac{v_i}{2}\right)^{2t_i+m_i} \tag{16}$$

$$\begin{gathered}\mathrm{M}^B = M^{R-N}\mathrm{q}^B(P,G)\\ \mathrm{q}^B(P,G) = \frac{t!(t+G)!}{(2t+G)!}\end{gathered} \tag{17}$$

3. *SCATTERING AMPLITUDE AND INTENSITY*

Using the postulate, power series expressions will be derived for both the scattering amplitude and the intensity. Let's first put an example with $N = 3$ frequencies in the Bragg regime, the final state being the first diffraction order ($G = 1$).

$$f = \sum_{i=1}^{N} m_i f_i \left\{ \begin{array}{c} f = m_1 f_1 + m_2 f_2 + m_3 f_3 = 1 f_1 + 0 f_2 + 0 f_3 \\ G = (m_1, m_2, m_3) = (1, 0, 0) \end{array} \right. \tag{18}$$

The following table provides the necessary data for applying the postulate. Values will be calculated up to order '5' and the Feynman diagrams along with the path clusters are illustrated. In the subsequent columns, the number of allowed paths is quantified: first for the Raman-Nath diffraction regime, and then, using the q relation, for the Bragg diffraction regime.

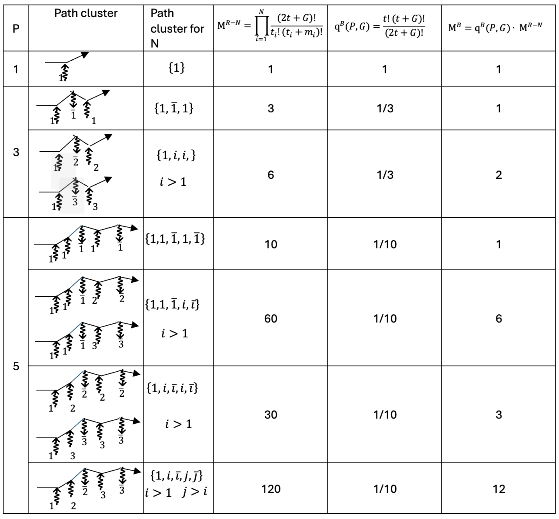

P	Path cluster	Path cluster for N	$M^{R-N} = \prod_{i=1}^{N} \frac{(2t+G)!}{t_i!\,(t_i+m_i)!}$	$q^B(P,G) = \frac{t!\,(t+G)!}{(2t+G)!}$	$M^B = q^B(P,G) \cdot M^{R-N}$
1		$\{1\}$	1	1	1
3		$\{1, \bar{1}, 1\}$	3	1/3	1
		$\{1, i, i,\}$ $i > 1$	6	1/3	2
5		$\{1,1,\bar{1},1,\bar{1}\}$	10	1/10	1
		$\{1,1,\bar{1},i,\bar{i}\}$ $i > 1$	60	1/10	6
		$\{1,i,\bar{i},i,\bar{i}\}$ $i > 1$	30	1/10	3
		$\{1,i,\bar{i},j,\bar{j}\}$ $i > 1 \quad j > i$	120	1/10	12

FIG. 5: Table of allowed combinations.

Applying the postulate generalized for N frequencies, it follows that:

First-order perturbation:

$$\boldsymbol{\Psi}_1^{(1)}(\boldsymbol{f}_1) = \frac{(-1)^0}{1!} \left(\frac{v_1}{2}\right)^1 = \left(\frac{v_1}{2}\right) \tag{19}$$

Third-order perturbation:

$$\Psi_1^{(3)}(f_1) = \frac{(-1)^1}{3!} \left[\left(\frac{v_1}{2}\right)^3 + \sum_{i=2}^{N} 2 \left(\frac{v_1}{2}\right) \left(\frac{v_i}{2}\right)^2 \right] \tag{20}$$

Fifth-order perturbation:

$$\boldsymbol{\Psi}_1^{(5)}(\boldsymbol{f}_1) = \frac{(-1)^2}{5!} \left\{ \left(\frac{v_1}{2}\right)^5 + \sum_{i=2}^{N} \left[6 \left(\frac{v_1}{2}\right)^3 \left(\frac{v_i}{2}\right)^2 + \right.\right.$$
$$\left.\left. +3 \left(\frac{v_1}{2}\right) \left(\frac{v_i}{2}\right)^4 \right] + \sum_{j=i+1}^{N} \sum_{i=2}^{N} \left[12 \left(\frac{v_1}{2}\right) \left(\frac{v_i}{2}\right)^2 \left(\frac{v_j}{2}\right)^2 \right] \right. \tag{21}$$

$$\Psi_1^B(f_1) = \Psi_1^{(1)}(f_1) + \Psi_1^{(3)}(f_1) + \Psi_1^{(5)}(f_1) \tag{22}$$

Now that the expression for the scattering amplitude for $G = 1$ and N frequencies in the Bragg regime has been obtained, the diffraction intensity can finally be expressed.

$$I_1^B = \Psi_1^B(f_1)\, \Psi_1^B(f_1) \tag{23}$$

Introducing equation (23):

$$\begin{aligned} I_1^B =& \Psi_1^{(1)}(f_1)\, \Psi_1^{(1)}(f_1) + 2\Psi_1^{(1)}(f_1)\, \Psi_1^{(3)}(f_1) + \\ &+ 2\Psi_1^{(1)}(f_1)\, \Psi_1^{(5)}(f_1) + \Psi_1^{(3)}(f_1)\, \Psi_1^{(3)}(f_1) \end{aligned} \tag{24}$$

Grouping by same orders:

$$I_1^B = \mathrm{I}_1^{(2)}(f_1) + \mathrm{I}_1^{(4)}(f_1) + \mathrm{I}_1^{(6)}(f_1) \tag{25}$$

III. STUDY OF EFFICIENCY CURVES

We want to study how the action of various frequencies, modeled by Feynman diagrams, affects the efficiency curves of AODs. Fig. 6 shows a typical efficiency response, where we can see two peaks corresponding to frequencies satisfying Bragg condition,

$$\eta_{\max} \equiv \sin^2\left(\frac{v}{2}\right). \tag{26}$$

As explained in section I.A, other frequencies i with Bragg mismatch have lower efficiencies, given by:

$$\eta_i = \eta_{\max} \cdot \mathrm{sinc}^2(\theta_i), \tag{27}$$

where $\theta_i = \frac{\Delta k_i L}{2}$ (section I.A and Fig. 3).

The curve can be flattened to have a homogeneous efficiency $\bar{\eta}$ by tuning the acoustic power P_{a_i} (or v_i) of each frequency to compensate for the decrease due to Bragg mismatch (except when one reaches saturation), that is:

$$\bar{\eta} = \sin^2\left(\frac{v_i}{2}\right) \cdot \mathrm{sinc}^2(\theta_i), \tag{28}$$

$$v_i = \frac{2\pi}{\lambda} \left[\frac{M_2 L}{2H} P_{a_i}\right]^{\frac{1}{2}}. \tag{29}$$

Here, L and H are the dimensions of the transducer and M_2 depends on the density and speed of the acoustic wave and on the index of refraction of light in the crystal.

Solving equations (27) and (28) for v_i gives: $v_i = 2 \cdot \arcsin\left(\sqrt{\frac{\bar{\eta}\cdot\eta_{\max}}{\eta_i}}\right)$. The weights v_i when considering single frequencies are shown in Fig. 7 (red).

Let's now consider that the N simultaneous frequencies interact by applying Feynman diagram; the efficiency η_i^{FD} for each frequency is then expressed as:

$$\eta_i^{\mathrm{FD}} = I_i(v_1, v_2, \ldots, v_i, \ldots, v_N) \cdot sinc^2(\theta_i) \qquad (30)$$

In order to ensure that all efficiencies are equal to $\bar{\eta}^{FD}$, an iterative process will be applied, starting by the values calculated previously $(v_1, v_2, \ldots, v_i, \ldots, v_N)$ to new corrected values $(\hat{v}_1, \hat{v}_2, \ldots, \hat{v}_i, \ldots, \hat{v}_N)$.

Please note that the number of frequencies considered, (N), depends on the target efficiency. Beyond a certain number of frequencies, the intensities exceed unity, making them physically meaningless. This marks the point of saturation, as explained in the appendix.

N = 10 ; f_i	$f_4 = 16$ **MHz**	$f_{13} = 61$ **MHz**	$f_{25} = 121$ **MHz**
η_i	0.8266	0.8034	0.9000
$\mathrm{sinc}^2\theta_{ai}$	0.9185	0.8927	1.0000
$v_i(\bar{\eta} = 0.5)$	1.6596	1.6912	1.5707
$I_i = I(v_1, \cdots, v_N)$	0.4523	0.46589	0.4145
η_i^{FD}	0.4155	0.4159	0.4145
$\hat{v}_i(\bar{\eta}^{FD} = 0.4)$	1.6329	1.6319	1.6353

TABLE I: Results for different frequencies f_i.

Table 1 lists the data necessary to obtain the final $\hat{v}_i$, which are related to the required acoustic powers to ensure a homogeneous efficiency. First, the values v_i were calculated by adjusting them to obtain $\bar{\eta} = 0.5$. This is the maximum efficiency achievable for 10 simultaneous frequencies, due to the saturation effect described earlier. To have higher efficiencies without saturation, the number of frequencies should be reduced.

Fig. 7 shows the final $\hat{v}_i$ values (blue) to correct for the inhomogeneities in efficiency of Fig.6, when applying 10 simultaneous frequencies using the Feynman diagram model, compared with the weights computed when the frequencies do not interact (red). We can see how, when the frequencies interact, smaller variations in acoustic powers are required to attain the same correction in efficiency; in other words, the effect of varying acoustic powers on efficiency homogeneity is more important when the frequencies interact than when single frequencies are considered. Even if simplified, in the future we plan to incorporate the Feynman model into experimental measurements to improve the procedure to flatten the curve.

IV. CONCLUSION

The research presented in this work advances the understanding and application of acousto-optic deflectors by incorporating a corpuscular model based on photon-phonon interactions. A key outcome of this approach is achieving more homogeneous intensity distributions across multiple diffraction points, which is critical for applications requiring precise and uniform light deflection.

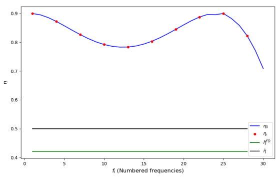

FIG. 6: Initial (η_i) and final ($\bar{\eta}$ and $\bar{\eta}^{FD}$) efficiencies applying the two models.

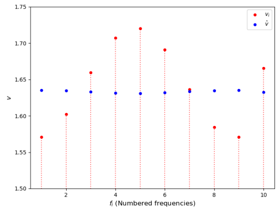

FIG. 7: v_i values when applying a single frequency (red) or all frequencies simultaneously (blue).

Through the integration of Feynman diagram-inspired models, the study successfully links quantum mechanics to classical wave interactions, offering novel insights into multi-frequency acousto-optic interactions. The findings are not only academically significant, but also have practical implications for optimizing light pattern generation in advanced optical systems, such as confocal microscopy and holography. By addressing both the theoretical and experimental aspects of AOD functionality, this work lays a strong foundation for future explorations into more efficient and versatile optical devices.

This research contributes to the broader field of photonics by bridging fundamental theory with technological innovation, emphasizing the importance of precise acoustic control.

Acknowledgments

I sincerely thank Prof. E. Martín for her dedicated mentorship, thoughtful advice, and constant encouragement, which have been crucial throughout the development of this work.

[1] M. Montes et al. "Programmable multiple-point illuminator, confocal filter, confocal microscope and method to operate said confocal microscope". Patent EP18382491.1 (2018).

[2] J. Xu, R. Stroud, *Acousto-Optic Devices: Principles, Design and Applications.* (J. Wiley & Sons, New York, 1992).

[3] S. Sun et al. "Collaborative optimization of phase and amplitude of composite signals for acousto-optic beam splitting technology". Opt. Express **32**: 31621-31632 (2024).

[4] M. Endres et al. "Atom-by-atom assembly of defect-free one-dimensional cold atom arrays". Science **354**: 1024-1027 (2016).

Preparació del manuscript del TFG amb LaTeX

Author: Antoni Bericat Vadell
Facultat de Física, Universitat de Barcelona, Diagonal 645, 08028 Barcelona, Spain.

Advisor: Estela Martín Badosa

Resum: Aquest treball explora els límits de rendiment dels desviadors acusto-òptics (AODs), utilitzant un model corpuscular inspirat en la mecànica quàntica per analitzar les interaccions entre fotons i fonons. L'objectiu és aconseguir una difracció de la llum homogènia en múltiples punts simultàniament, optimitzant l'eficiència de difracció mitjançant la teoria de diagrames de Feynman. Els resultats d'aquest estudi contribueixen al desenvolupament de sistemes avançats en òptica fotònica, com la microscòpia confocal i l'holografia, oferint una millor comprensió de les interaccions multifreqüència i maximitzant l'homogeneïtat en patrons de llum complexos. **Paraules clau:** Acusto-òptica, fotons, fonons, difracció, diagrames de Feynman, eficiència òptica.
ODSs: Aquest TFG està relacionat amb els Objectius de Desenvolupament Sostenible (SDGs)

Objectius de Desenvolupament Sostenible (ODSs o SDGs)

1. Fi de la es desigualtats		10. Reducció de les desigualtats	
2. Fam zero		11. Ciutats i comunitats sostenibles	
3. Salut i benestar		12. Consum i producció responsables	
4. Educació de qualitat	X	13. Acció climàtica	X
5. Igualtat de gènere		14. Vida submarina	
6. Aigua neta i sanejament		15. Vida terrestre	
7. Energia neta i sostenible	X	16. Pau, justícia i institucions sòlides	
8. Treball digne i creixement econòmic		17. Aliança pels objectius	
9. Indústria, innovació, infraestructures	X		

El contingut d'aquest TFG, part d'un grau universitari de Física, es relaciona amb l'ODS 4, i en particular amb la fita 4.4, ja que contribueix a l'educació a nivell universitari i l'avanç del coneixement científic. També es pot relacionar amb l'ODS 7, fita 7.2, ja que el treball explora l'optimització de sistemes acusto-òptics amb potencial per millorar l'eficiència energètica. A més, s'alinea amb l'ODS 9, fita 9.5, perquè fomenta la innovació tecnològica en dispositius fotònics i el desenvolupament d'infraestructures òptiques avançades. Finalment, es vincula amb l'ODS 13, fita 13.4, ja que promou l'educació i l'ús de tecnologies per a la mitigació i adaptació al canvi climàtic.

V. SUPPLEMENTARY MATERIAL

A. Intermodulation

The Feynman diagram model allows us to calculate the intensities for final states composed of several frequencies of the existing N: $f = \sum_{i=1}^{N} m_i f_i$. The ones to be treated here will be $f = f_1 - f_2$ for the order $G = 0$ and, for $G = 1$, the so-called two-tone intermodulation $f = 2f_1 - f_2$.

P	Path cluster	Path cluster para N	$M^{R-N} = \prod_{i=1}^{N} \frac{(2t+G)!}{t_i!\,(t_i+m_i)!}$	$q^B(P,G) = \frac{t!\,(t+G)!}{(2t+G)!}$	$M^B = q^B(P,G) \cdot M^{R-N}$
2	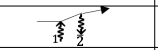	$\{1,\bar{2}\}$	2	1/2	2
4	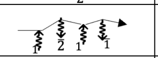	$\{1,\bar{2},1,\bar{1},\}$	12	1/6	2
	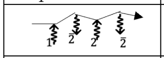	$\{1,\bar{2},2,\bar{2}\}$	12	1/6	2
	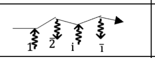	$\{1,\bar{2},i,\bar{\imath},\}$ $i>1$	24	1/6	4
6	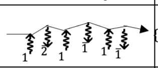	$\{1,\bar{2},1,\bar{1},1,\bar{1}\}$	60	1/20	3
	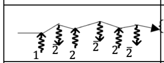	$\{1,\bar{2},2,\bar{2},2,\bar{2}\}$	60	1/20	3
	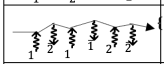	$\{1,\bar{2},1,\bar{1},2,\bar{2}\}$	180	1/20	9
	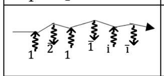	$\{1,\bar{2},1,\bar{1},i,\bar{\imath}\}$ $i>1$	360	1/20	18
	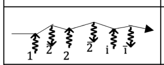	$\{1,\bar{2},2,\bar{2},i,\bar{\imath}\}$ $i>1$	360	1/20	18
	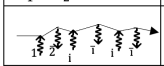	$\{1,\bar{2},i,\bar{\imath},i,\bar{\imath}\}$ $i>1$	180	1/20	9
	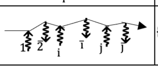	$\{1,\bar{2},i,\bar{\imath},j,\bar{\jmath}\}$ $i>1$	720	1/20	36

FIG. 8: Table of allowed combinations.

Applying the postulate (16):

$$\Psi_0^B(f_1-f_2) = \Psi_2^{(2)}(f_1-f_2)+\Psi_2^{(4)}(f_1-f_2)+\Psi_2^{(6)}(f_1-f_2) \tag{31}$$

$$I_0^B(f_i-f_j) = \left|\Psi_0^B(f_i-f_j)\right|^2 \tag{32}$$

B. Saturation

Next, in order to find the zero-order intensity, we will sum all the intermodulations of this order with that of the final state (0): $I_0^B(0)$. Once this is done, we will calculate the first-order intensity. We will apply this to a specific case where $v_i = v = 0.8$, and using the table and the graph, we will conclude that from a certain number of frequencies, the total intensity exceeds unity, indicating that saturation has been reached. The interpretation could be that in the photon-phonon interaction, the density of phonons surpasses that of photons.

P	Path cluster	Path cluster for N	$M^{R-N} = \prod_{i=1}^{N} \frac{(2t+G)!}{t_i!\,(t_i+m_i)!}$	$q^B(P,G) = \frac{t!\,(t+g)!}{(2t+G)!}$	$M^B = q^B(P,G) \cdot M^{R-N}$
0	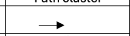	$\{0\}$	1	1	1
2	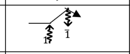	$\{1,\bar{1}\}$	2	1/2	1
4	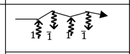	$\{i,\bar{\imath},i,\bar{\imath}\}$	6	1/6	1
	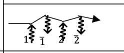	$\{i,\bar{\imath},j,\bar{\jmath}\}$ $j>i$	24	1/6	4
6	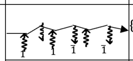	$\{1,\bar{1},1,\bar{1},1,\bar{1},\}$	20	1/20	1
	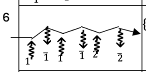	$\{1,1,\bar{1},1,\bar{1},i,\bar{\imath}\}$ $i>1$	180	1/20	9
	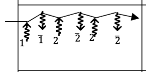	$\{i,i,j,\bar{\jmath},j,\bar{\jmath}\}$ $j>i$	180	1/20	9
	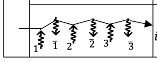	$\{i,\bar{\imath},j,\bar{\jmath},k.\bar{k},\}$ $i>1$ $j>i$	720	1/20	36

FIG. 9: Table of allowed combinations.

Applying the postulate (16):

$$\Psi_0^B(0) = \Psi_0^{(0)}(0) + \Psi_0^{(2)}(0) + \Psi_0^{(4)}(0) + \Psi_0^{(6)}(0) \tag{33}$$

$$I_0^B(0) = \left|\Psi_0^B(0)\right|^2 \tag{34}$$

	V=0.8 N=14	V=0.8 N=16	V=0.8 N=18	V=0.8 N=19
$\Psi_0^B(0)$	0.1990	0.1219	0,0491	0.0137
$I_0^B(0)$	0.0397	0.0140	0.0024	0.00019
$\Psi_0^B(f_i-f_j)$	-0.0412	-0.0383	-0.0362	-0.0355
$I_0^B(f_i-f_j)$	0.00169	0.00146	0.001312	0.00126
$\Psi_1^B(f_i)$	0.2019	0.1880	0.1791	0.0176
$I_1^B(f_i)$	0.0407	0.0355	0.0321	0.031
$\Psi_1^B(2f_i-f_j)$	-0.004	-0.003	-0.00204	-0.0015
$I_1^B(2f_i-f_j)$	1.67 E-5	9,43 E-6	4.19 E-6	2.36 E-6
$I_0^B = I_0^B(0) + N(N-1)I_0^B(f_i-f_j)$	0,3487	0.3670	0.4039	0.431
$I_1^B = N \cdot I_1^B(f_i) + N(N-1) \cdot I_1^B(2f_i-f_j)$	0.5739	0.5705	0.579	0.588
$I^B = I_0^B + I_1^B$	0.922	0.937	0,983	1.019

FIG. 10: Calculated intensities for $v = 0.8$ and different values of N.

In the table we observe that, starting from $N = 18$, the total intensity, which is normalized, exceeds unity.